OXFORD
SOT | Society of Toxicology
academic.oup.com/toxsci

Toxicological Sciences, 2024, **198(2)**, 260–272
https://doi.org/10.1093/toxsci/kfae009
Advance Access Publication Date: January 24, 2024
Research article

Developmental toxicity of pyriproxyfen induces changes in the ultrastructure of neural cells and in the process of skull ossification

Maico Roberto Luckmann, Méllanie Amanda Silva Ferreira, Norma Machado da Silva, Evelise Maria Nazari *

Department of Cell Biology, Embryology and Genetics, Federal University of Santa Catarina, Florianópolis, Santa Catarina, 88040-900, Brazil

*To whom correspondence should be addressed. E-mail: evelise.nazari@ufsc.br.

Abstract

Some studies relate the use of pyriproxyfen (PPF) in drinking water with damage to embryonic neurodevelopment, including a supposed association with cases of microcephaly. However, the effects on neural cells and skull ossification in embryos remain unclear. This study aims to investigate the effects of PPF on the structure and ultrastructure of brain cells and its influence on the skull ossification process during embryonic development. Chicken embryos, used as an experimental model, were exposed to concentrations of 0.01 and 10 mg/l PPF at E1. The findings demonstrated that PPF led to notable ultrastructural alterations such as reduced cilia and microvilli of ependymal cells and damage to mitochondria, endoplasmic reticulum, Golgi bodies, and cell membranes in neural cells. The frequency of changes and the degree of these cell damage between the forebrain and midbrain were similar. PPF induced a reduction in *fox3* transcript levels, specific for differentiation of neurons, and a reduction in the NeuN protein content related to mature neurons and dendritic branches. PPF impacted the ossification process of the skull, as evidenced by the increase in the ossified area and the decrease in inter-bone spacing. In conclusion, this study highlights the ability of PPF to affect neurodevelopmental processes by inducing ultrastructural damage to neural cells, concomitant with a reduction in NeuN and fox3 expression. This detrimental impact coupled with deficiencies in skull ossification can prevent the proper growth and development of the brain.

Keywords: head ossification; forebrain and midbrain; neural cells; embryotoxicity; cytotoxicity.

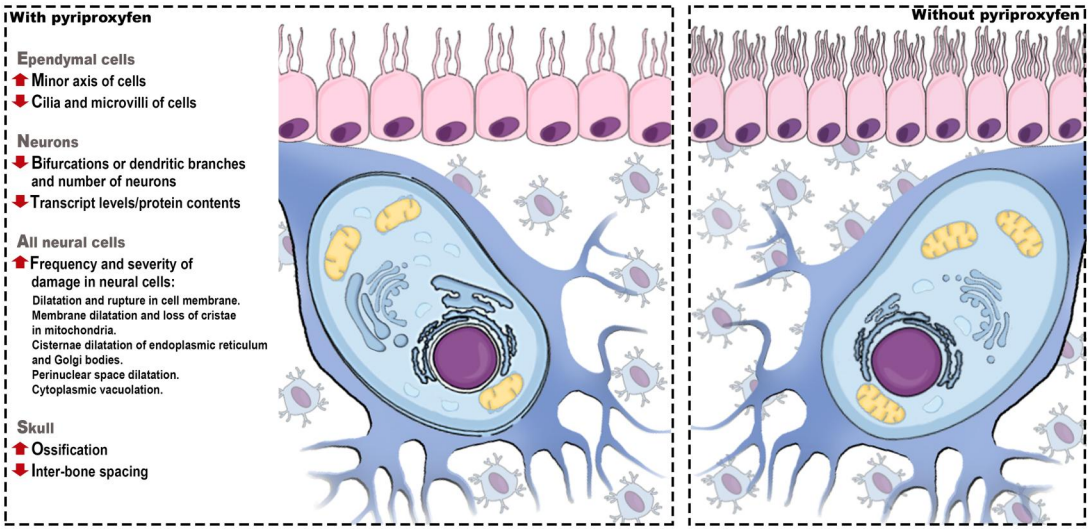

Graphical Abstract

Microcephaly is a congenital anomaly in which a reduction in head circumference is observed, and the brain does not grow properly (Mochida, 2009; Opitz and Holt, 1990; Woods and Parker, 2013). Worldwide, it is considered a rare condition, and the incidence usually varies from 1.3 to 150 per 100 000 live births (Becerra-Solano *et al.*, 2021; Passemard *et al.*, 2013). However, the estimated incidence of microcephaly may vary due to differences in the definition of reference cephalic measurements and the target population (DeSilva *et al.*, 2017). Conventional risk factors are well documented for microcephaly, such as genetic alterations,

Zika virus infection, and exposure to toxic substances (Becerra-Solano *et al.*, 2021; Brassier *et al.*, 2012).

Another possible risk factor proposed for microcephaly is the use of the larvicide pyriproxyfen (PPF) in drinking water reservoirs to control the *Aedes aegypti* mosquito in areas with a high incidence of diseases transmitted by this vector (WHO, 2006). In this particular scenario, pregnant women may be exposed to significant amounts of PPF, representing a concern for the development of embryos, especially here, the correct development of the central nervous system. According to the WHO-recommended classification of agrochemicals by hazard, PPF is classified as unlikely to present an acute hazard in normal use (WHO, 2020). However, as it is a highly lipophilic molecule, there is a possibility that PPF accumulates in the lipid portions of the cells (PubChem, 2023).

Although it is not possible to determine the exact amount and duration of a disruptive toxic agent to induce damage to the nervous system (Becerra-Solano *et al.*, 2021), it is known that the developing nervous system is particularly more vulnerable to the harmful effects of toxic substances due to its immaturity of the blood-brain barrier and the intricate mechanisms involved in its formation (Liu *et al.*, 2016; Saunders *et al.*, 2012). In general, genetic and other biological factors, in addition to physical and chemical environmental factors, can interfere with essential processes such as neuronal proliferation and brain growth (Fritsche *et al.*, 2018; Gilmore and Walsh, 2013). Therefore, interruption in neurogenesis, interfering with neural proliferation (Woods *et al.*, 2005), differentiation (Juraver-Geslin and Durand, 2015), migration (Sarnat and Flores-Sarnat, 2002), DNA damage repair (Gilmore and Walsh, 2013), and apoptosis (Dekkers *et al.*, 2013) during the developmental stages, including postnatal growth, can result in central nervous system damage, such as microcephaly (Passemard *et al.*, 2013). Furthermore, the influence of toxic substances on the skull ossification process may result in premature fusion of sutures between bone plates, and associated with congenital anomalies can compromise cognitive development (Mattigk, 1989; Ross, 1993).

Considering developmental processes, research involving sublethal concentrations of PPF revealed significant impacts on the nervous system of nontarget vertebrate organisms. Direct exposure to PPF in the developing nervous system caused morphological changes in the body and head in zebrafish (Azevedo-Linhares *et al.*, 2018; Truong *et al.*, 2016), morphological changes in the cell layers of the brain in chicken embryos (Luckmann *et al.*, 2021), mitochondrial damage and changes in acetylcholinesterase in zebrafish (Azevedo *et al.*, 2021), production and release of reactive oxygen species and depletion of antioxidant enzymes in the nervous system in freshwater fish (Li *et al.*, 2022) among other scarce reports. These few studies support the first associations between PPF and neurodevelopmental damage in vertebrates. In this way, this study reinforces and advances investigations on the impact of exposure to PPF on the development of the central nervous system. The proposed hypothesis is that PPF impairs brain growth and development, as it affects the integrity and differentiation of neural cells and skull ossification.

Materials and methods

Experimental design

Fertilized eggs of *Gallus domesticus* (Poultry Laboratory of the Federal University of Santa Catarina/UFSC, Brazil) were incubated according to parameters defined by Müller *et al.* (2008). After 24 h of incubation (first embryonic day, E1), 2 concentrations of PPF (Sigma-Aldrich), 0.01 and 10 mg/l (Luckmann *et al.*, 2021) were administered *in ovo* in a volume of 50 µl. Control embryos (0.00 mg/l PPF) received 50 µl of vehicle solution, DMSO diluted in 0.9% saline solution. The embryos remained exposed until it was possible to define cell layers in the forebrain and midbrain (Lavail and Cowan, 1971) and to identify several bones of the head in an advanced process of ossification (Couly *et al.*, 1993). After exposure, the embryos were anesthetized and removed from the eggs according to the procedure described by Müller *et al.* (2008) and approved by the Federal University of Santa Catarina Ethics Committee (n° 5843231018).

Transmission and scanning electron microscope

Fragments of forebrain and midbrain were fixed in 2.5% glutaraldehyde (Electron Microscopy Sciences), 4% paraformaldehyde (PFA), and 0.1 M sodium cacodylate buffer (Sigma-Aldrich). Samples were post-fixed with 1% osmium tetroxide (Sigma-Aldrich), washed in 0.1 M sodium cacodylate buffer and dehydrated in acetone series (30%–100%), intended for transmission and scanning electron microscopies (TEM and SEM).

For TEM, the samples ($n = 3$ brains/PPF concentration) were infiltrated with Spurr resin (Electron Microscopy Sciences), semithin sections (700 nm) were stained with 1% toluidine blue, and ultrathin sections (60–90 nm) were stained with 5% uranyl acetate (Electron Microscopy Sciences) followed by 1% lead citrate (Sigma-Aldrich). Analysis and micrograph capture were performed in a JEOL JEM-1011 TEM at 80 kV ($n = 36$ micrographs/brain vesicle; 1 cell was visible per micrograph) (Supplementary Table 1). The frequency of alterations in subcellular compartments was assessed through the occurrence in cells, represented by scores: – (0%, absent), + (1%–25%), ++ (26%–50%), +++ (51%–75%), ++++ (76%–100%).

To access the degree of cell damage, the cell index (I_{cell}) (Bernet *et al.*, 1999 modified by De Melo *et al.*, 2019) was calculated, using the formulae Σ_{alt} $(a \cdot w)$, where (alt) each alteration; (a) score value based on the frequency of occurrence: 0 (0%, no damage), 1 (1%–20%), 2 (21%–40%), 3 (41%–60%), 4 (61%–80%), and 5 (81%–100%); and (w) importance factor based on level of damage severity according to its degree of reversibility: (1) minimal importance, easily reversible alterations; (2) moderate importance, alterations that are generally reversible; and (3) marked importance, irreversible alterations that may involve total or partial loss of the subcellular compartment (Table 1).

For SEM, the samples ($n = 3$ brains/PPF concentration) were dried at the critical point and coated with gold. Image analysis and capture were performed using a JEOL JSM-6390LV SEM. The length of the major and minor axes in the ependymal cells was measured with ImageJ (NIH) ($n = 6$ micrographs/brain vesicle; with approximately 18 cells visible in each micrograph) (Supplementary Table 1). The total area of cilia and microvilli of ependymal cells was analyzed by optical density with ImageJ ($n = 6$–8 micrographs/brain vesicle). Medio-lateral and dorso-ventral areas of the forebrain and midbrain were used for electron microscopic analyses and immunohistochemistry.

RT-qPCR for neuronal and glial genes

Total RNA from the whole brain ($n = 9$ brains/concentration) (Supplementary Table 2) was extracted using TRIzol reagent (Sigma-Aldrich). The RNA samples were submitted to treatment with DNAse I (Promega), and their integrity was evaluated using 1% agarose gel electrophoresis with GelRed (Start BioScience). RNA concentration and purity were determined using a Thermo Scientific NanoDrop 1000 spectrophotometer, where absorbance ratio > 1.8 of RNA samples at 260 and 280 nm (A260/280) was

Table 1. Importance factor for the reversibility of damage in subcellular compartments of the brain of *Gallus domesticus* embryos exposed to pyriproxyfen

Importance factor and damage reversibility	Subcellular compartments alterations	References
(1) Easily reversible	Dilatation of endoplasmic reticulum cisterns Dilatation of Golgi cisterns Dilatation of cell membranes	Whetsell and Bunge (1969); Escande-Geraud *et al.* (1988); Boissy *et al.* (1991); Radulescu *et al.* (2007)
(2) Generally reversible	Cytoplasmic vacuolization Dilatation of mitochondrial membrane Dilatation of perinuclear space	Hackenbrock (1966); Henics and Wheatley (1999); Shaiken and Opekun (2014)
(3) Irreversible	Cell membrane rupture Loss of mitochondrial cristae	Röth *et al.* (1980); Misfeld *et al.* (1998)

considered adequate for cDNA synthesis. cDNA was synthesized from RNA samples (1 µg) using oligo(dT) with GoScript Reverse Transcription System (Promega). For the qPCR technique, GoTaq qPCR Master Mix (Promega) was used. qPCR reaction (10 µl) with 0.3 µM primers was performed using the HT 7900 Fast Real-Time PCR System. Primers *fox3* (F: TTTTCAATGAGCGGGGCTCCAAGG; R: CAGCTTCCAGCCGTTAGTGTAGGG) were designed for this analysis, *gfap* (F: TGTCCCTGTGCAGAGCTT; R: CTCCTTGTGCTCCTGCTT) and *tubb3* (F: CTTCCTGCATTGGTACACG; R: GACTCCTCCTCAT CATCCTC) were designed by Cecchini *et al.* (2019), and *vim* (F: GGAACAATGATGCCCTGC; R: GCAAAATTCTCCCTCCATTTCAC) were designed by Olias *et al.* (2014). Normalization of transcribed genes was performed using glyceraldehyde-3-phosphate dehydrogenase (*gapdh*, F: AGTCATCCCTGAGCTGAATG; R: AGGA TCAAGTCCACAACACG) (Sanzo and Tuan, 1998). The same procedure was followed for the negative control, except that the biological samples were replaced with RNA-free water. The melting curves were analyzed to evaluate the specificity of the primers used in the qPCR. The ΔΔCt was calculated for each sample, and relative levels of transcripts were calculated by the $2^{-\Delta\Delta Ct}$ method (Livak and Schmittgen, 2001).

Immunohistochemistry for neuronal and glial proteins

The brains ($n = 3$ brains/concentration) were fixed in 4% formaldehyde, embedded in paraffin, and sectioned in a transverse plane at 6 µm. Brain sections were deparaffinized and washed with buffered solution and then with bovine serum albumin (BSA) according to the protocol used by Kobus *et al.* (2013). Sections were incubated overnight with the rabbit IgG1 anti-vimentin (1:100; Chemicon International) and mouse IgG1 anti-NeuN (1:100; Chemicon International) to identify glial cells and mature neuronal cells, respectively. Then, the sections were incubated with antimouse IgG (1:100; Sigma-Aldrich). The sections were revealed with 3,3′- diaminobenzidine (DAB; Sigma-Aldrich). The negative control followed the same procedure, except that the primary antibody was replaced with phosphate-buffered saline (PBS) 0.1 M. Positive cells were quantified with Weibel M-42 graticule (Weibel No. 2 Tonbridge, United Kingdom) coupled to a light microscope. Ten random, nonoverlapping visual fields per brain vesicle were evaluated (Supplementary Table 1). To calculate positive cells per area (mm^2), the formula ([number of cells/36.36 mm^2] × 0.0004) was used (Mandarim-de-Lacerda, 2003).

Golgi staining for neuronal cells

Brains ($n = 6$ brains/concentration) were fixed in 4% PFA, placed in Golgi-Cox solution, and stored at room temperature in the dark. Then, the brains were transferred to a sucrose cryoprotective solution at 5%, 15%, and 30%. The samples were embedded in Tissue-Tek (Sakura), and serial 100 µm sections were obtained in a Thermo Scientific HM525 NX cryostat microtome. Sections on histological slides were made alkaline in ammonium hydroxide, fixed in Kodak rapid fixer (Sigma-Aldrich), dehydrated in a graded series of ethanol concentrations (50%–100%), clarified in xylol and finished with Entelan (Merk, Germany). The area, length of dendrites, and number of bifurcations were analyzed with ImageJ ($n = 25$ micrographs/brain vesicle) (Supplementary Table 1).

Histochemical reactions for cartilage and bone

Heads in E10 ($n = 6$ heads/PPF concentration) and E15 ($n = 6$ heads/PPF concentration) were washed in 1× PBS pH 7.0, and then submitted to Alcian blue solution for cartilage staining. Then washings were performed with 100% ethanol. For bone staining, the heads were placed in Alizarin red solution and then, submitted to the tissue bleaching with Mall's solution (potassium hydroxide + glycerol + Milli-Q water) (Mall, 1906). Images were analyzed with ImageJ to calculate area of bones and interbone spacing (Supplementary Table 1). The squamosal, frontal, parietal, and supraoccipital head bones were analyzed based on the description of Couly *et al.* (1993).

Statistical analysis

The normality of the data was assessed by the Shapiro-Wilk test. One-way ANOVA was performed for parametric data, followed by Tukey's post hoc test. The Kruskal-Wallis test was performed for nonparametric data, followed by Dunn's post hoc test. Statistical tests were performed using the GraphPad Prism 9 program. The data were expressed as mean ± SEM (standard error of the mean).

Results

PPF interferes with the ultrastructure of ependymal cells

The analysis of the ependymal layer of the forebrain shows that there was a reduction of area of the cilia and microvilli in groups exposed to PPF (Figure 1; Supplementary Table 3). The total area of cilia and microvilli of ependymal cells decreased in the groups exposed to 10 mg/l PPF (26 582 μm^2 ± 6159; $p < .001$) and 0.01 mg/l PPF (36 430 μm^2 ± 2401; $p < .01$), compared with control (57 342 μm^2 ± 2702) (Figs. 1C and 1E). Regarding cell axis length, there was only a reduction in the minor axis of groups exposed to 0.01 mg/l PPF (2.87 µm ± 0.09; $p < .05$), compared with control (3.19 µm ± 0.09) (Figs. 1B and 1D). No changes were observed in the major axis of the ependymal cells.

Ependymal cells in the forebrain of groups exposed to PPF exhibited a high frequency of alterations in their subcellular compartments (Figs. 1F–H, Table 2). These alterations included increased cell membrane dilatation and rupture, cytoplasmic vacuolation, loss of mitochondrial cristae, as well as dilatation of

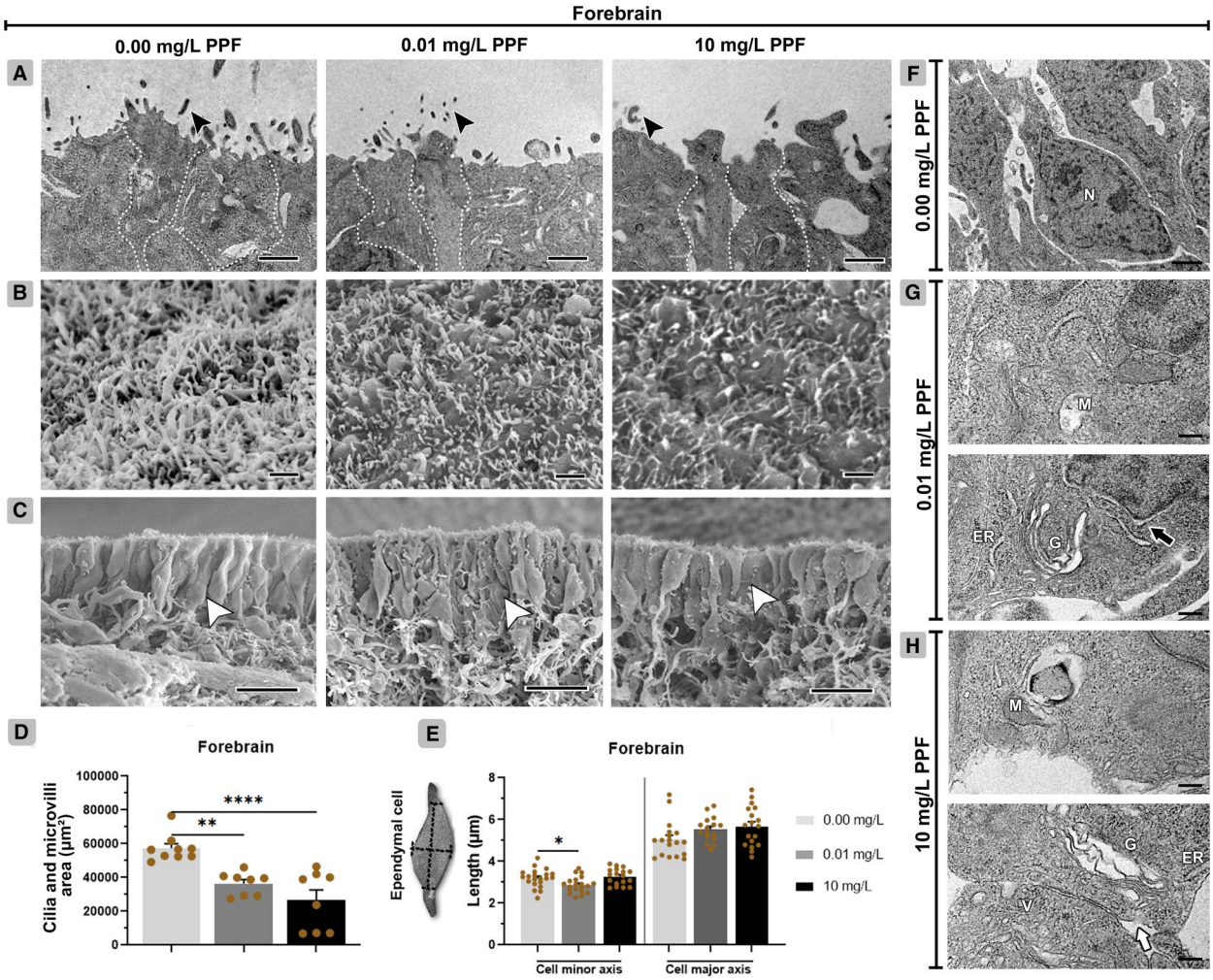

Figure 1. Ependymal cells of the forebrain in *Gallus domesticus* E10 embryos exposed to pyriproxyfen. A, Ultrastructure of ependymal cells showing cell body (dashed line delineates the cells) and cilia and microvilli (black arrowhead). B, Top view of the ependymal layer showing cilia and microvilli. C, Lateral view of the ependymal layer (white arrowhead). D, Area of cilia and microvilli in ependymal cells ($n = 3$ brains/6 micrographs/PPF concentration) shown in images (B). E, Measurement of ependymal cell axes, shown in images (C). F, Cell architecture of groups exposed to 0.00 mg/l PPF. G and H, Exposed groups (0.01 and 10 mg/l PPF) showing ependymal cells with cell membrane rupture (white arrow), perinuclear space dilatation (black arrow), Golgi bodies, and endoplasmic reticulum with cisternae dilatation, mitochondria with loss of cristae, and cytoplasmic vacuolization. ER, endoplasmic reticulum; G, Golgi bodies; M, mitochondria; N, nucleus; V, vacuolation. Scale bar in A, B, and F = 1 µm; in C = 10 µm; in G, H = 0.2 µm. Mean ± standard error of the mean (SEM). * $p < .05$, ** $p < .01$, **** $p < .0001$.

Table 2. Frequency of alterations in the subcellular compartments of neural cells in the forebrain and midbrain of *Gallus domesticus* E10 embryos exposed to pyriproxyfen.

		Forebrain			Midbrain		
Cell structure	**Alterations**	**0.00 mg/l**	**0.01 mg/l**	**10 mg/l**	**0.00 mg/l**	**0.01 mg/l**	**10 mg/l**
Cell membranes	Membrane dilatation	+	++	+	+	++	++
	Membrane rupture	+	++	+	+	++	+++
	Cytoplasmic vacuolation	+	++	+++	+	++	++
Mitochondria	Membrane dilatation	+	++	++	+	+++	++
	Loss of cristae	+	+	+++	+	++	++
Nucleus	Perinuclear space dilatation	+	+++	++	+	+++	++++
Endoplasmic reticulum	Cisternae dilatation	+	++	+++	+	+++	++
Golgi bodies	Cisternae dilatation	-	+	+++	+	+	++

Frequency: – (0%), + (1%–25%), ++ (26%–50%), +++ (51%–75%), ++++ (76%–100%); $n = 3$ brains/12 micrographs per brain vesicle/PPF concentration.

the perinuclear space, Golgi cisternae, and endoplasmic reticulum (ER) cisternae.

The total area of cilia and microvilli of the midbrain ependymal cells also decreased in the groups exposed to 10 mg/l PPF (34 444 µm^2 ± 3141; $p < .01$) and 0.01 mg/l PPF (40 502 µm^2 ± 2401; $p < .05$), compared with control (56 317 µm^2 ± 2547) (Figs. 2B and 2D). There was an increase in the minor axis of the group exposed to 10 mg/ PPF (3.72 µm ± 0.12; $p < 0.01$) compared with

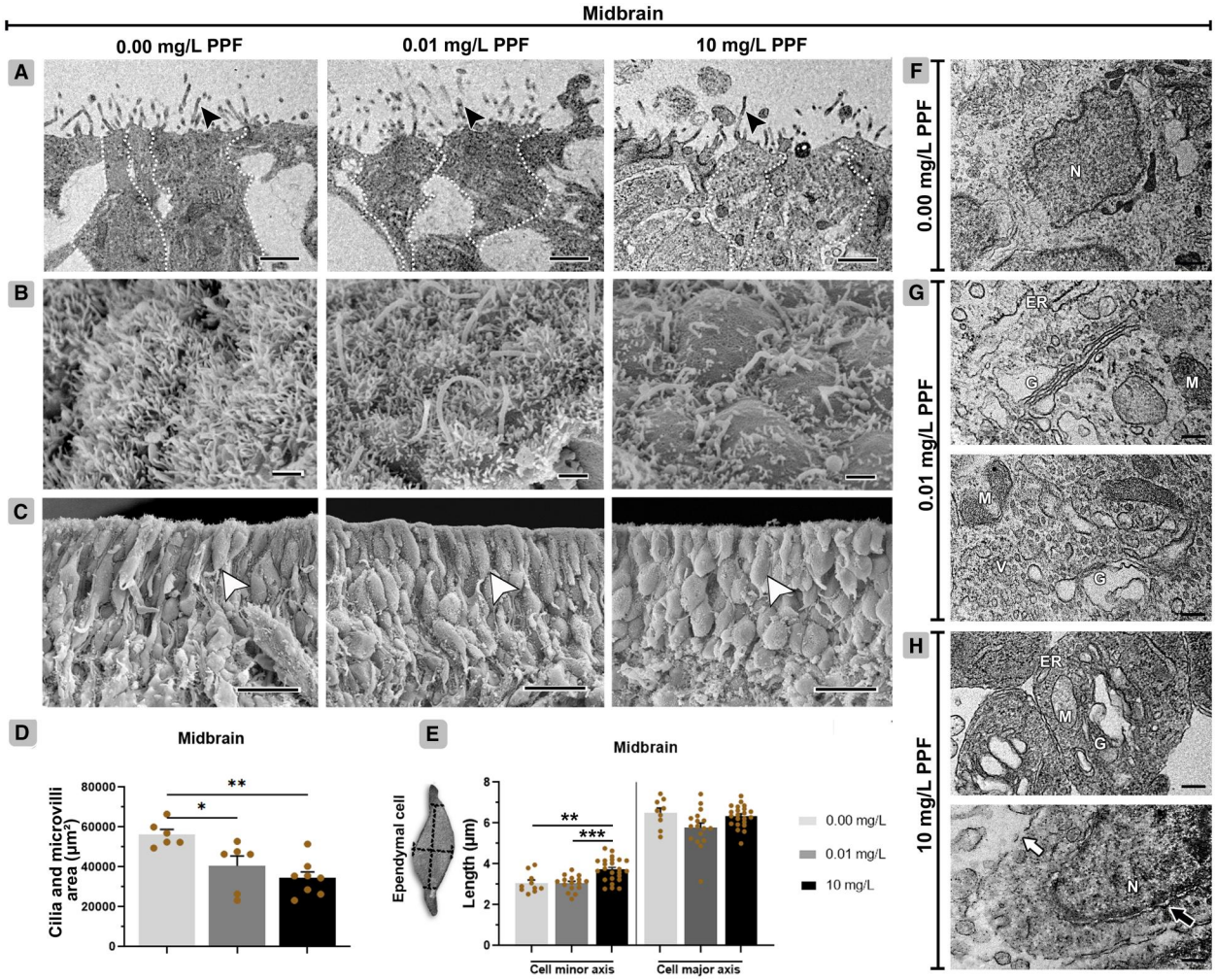

Figure 2. Ependymal cells of the midbrain in *Gallus domesticus* E10 embryos exposed to pyriproxyfen. A, Ultrastructure of ependymal cells showing cell body (dashed line delineates the cells), and cilia and microvilli (black arrowhead). B, Top view of the ependymal layer showing cilia and microvilli. C, Lateral view of the ependymal layer (white arrowhead). D, Area of cilia and microvilli in ependymal cells ($n = 3$ brains/6 micrographs/PPF concentration) shown in images (B). E, Measurement of ependymal cell axes, shown in images (C). F Cell architecture of groups exposed to 0.00 mg/l PPF. G and H, Exposed groups (0.01 and 10 mg/l PPF) showing ependymal cells with cell membrane rupture (white arrow), perinuclear space dilatation (black arrow), Golgi bodies, and endoplasmic reticulum with cisternae dilatation, mitochondria with loss of cristae, and cytoplasmic vacuolization. ER, endoplasmic reticulum; G, Golgi bodies; M, mitochondria; N, nucleus; V, vacuolation. Scale bar in A, B, and F = 1 µm; in C = 10 µm; in G, H = 0.2 µm. Mean ± standard error of the mean (SEM). * $p < .05$, ** $p < .01$.

control (3.06 µm ± 0.15) (Figs. 2C and 2E). Also, no differences were observed in the major axis of the ependymal cells between groups.

Ependymal cells in the midbrain of groups exposed to PPF exhibited a high frequency of alterations in their subcellular compartments (Figs. 2F–H, Table 2). These alterations also included increased cell membrane dilatation and disruption, cytoplasmic vacuolation, loss of mitochondrial cristae, as well as dilatation of the perinuclear space, Golgi cisternae, and endoplasmic reticulum cisternae.

Effects of PPF on neural subcellular compartments

The frequency of subcellular alterations of neural cells increased in the 10 mg/l PPF (Figs. 3G–I and 3P–R) and 0.01 mg/l PPF (Figs. 3D–F and 3M–O) groups when compared with control (Figs. 3A–C and 3J–L). Results were similar in the forebrain and midbrain. High frequencies of cell membrane dilatation and rupture were observed, as well as vacuolation, mitochondrial membrane dilatation, and loss of mitochondrial cristae (Figure 3, Table 2). Additionally, dilatation of the perinuclear space, Golgi cisternae, and endoplasmic reticulum cisternae was observed.

The calculated cell index (I_{cell}) was higher in neural cells (ependyma, glia, and neuron) from embryos exposed to PPF, regardless of forebrain, and midbrain (Figure 4, Table 1, Supplementary Table 3). The I_{cell} showed significant differences in subcellular compartments in the forebrain in groups exposed to 10 mg/l PPF (34.33 I_{cell} ± 5.36; $p < .05$) and 0.01 mg/l PPF (31.00 I_{cell} ± 4.51; $p < .05$) compared with control (7.33 I_{cell} ± 3.38). In the midbrain, significant differences were also observed in the subcellular compartments of groups exposed to 10 mg/l PPF (40.33 I_{cell} ± 4.70; $p < .001$) and 0.01 mg/l PPF (33.67 I_{cell} ± 1.45; $p < .01$) compared with control (5.33 I_{cell} ± 3.18).

Effect of PPF on neural cell content and dendritic arborization

Glial cells were immunolocalized in all cell layers of the forebrain and midbrain (Figs. 5A–F; Supplementary Table 3). No significant differences were observed for vimentin protein content between

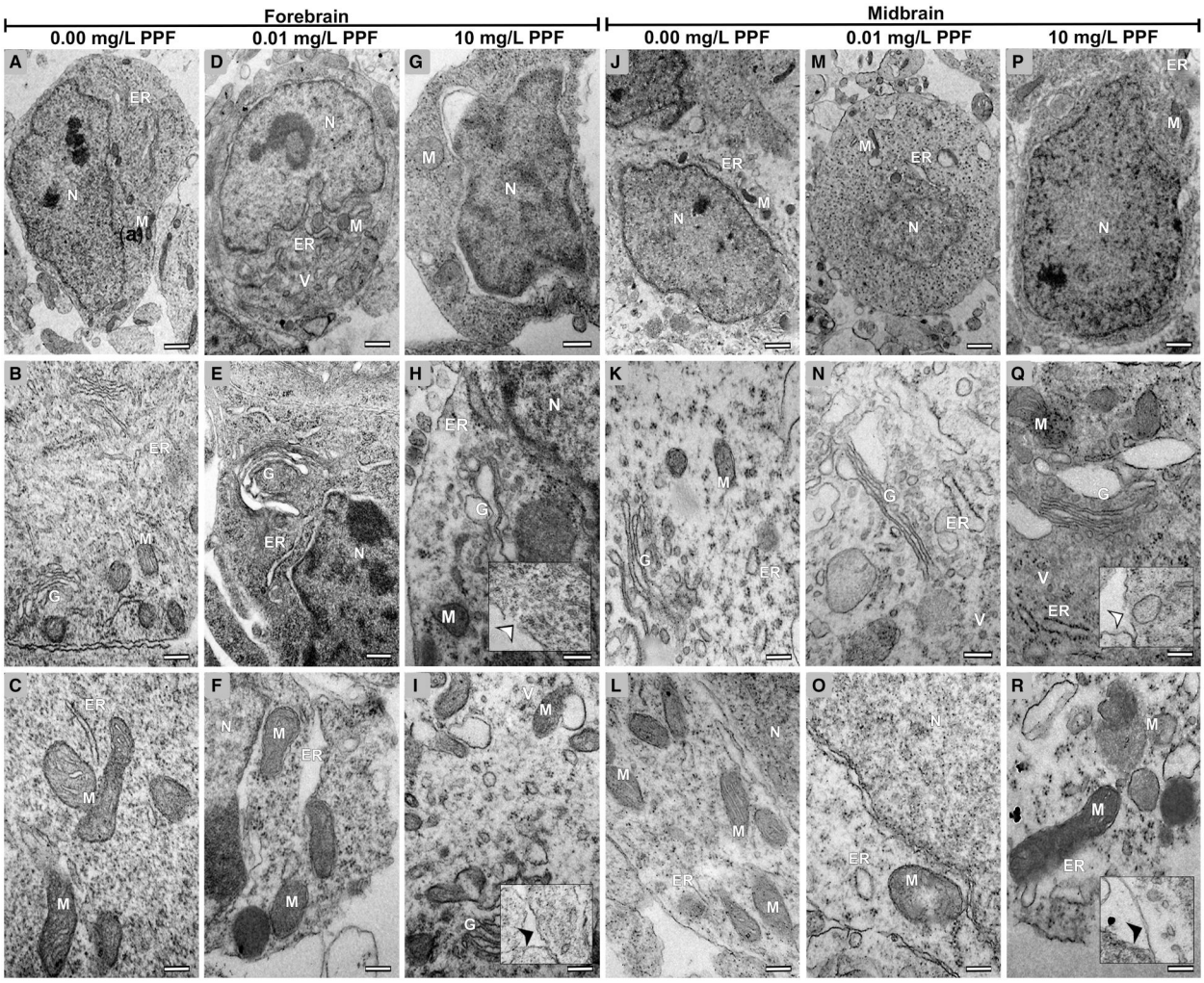

Figure 3. Neural cells from the forebrain and midbrain of *Gallus domesticus* E10 embryos exposed to pyriproxyfen. A–C and J–L, Cellular architecture of groups exposed to 0.00 mg/l PPF. D–I and M–R, Exposed groups (0.01 and 10 mg/l PPF) showing neural cells with cell membrane rupture (white arrowhead in inserts) and cell membrane dilatation (black arrowhead in inserts), Golgi bodies, and endoplasmic reticulum with cisternae dilatation, mitochondria with membrane rupture and loss of cristae, and increased cytoplasmic vacuolation. ER, endoplasmic reticulum; G, Golgi bodies; M, mitochondria; N, nucleus; V, vacuolation. $n = 3$ brains/30 micrographs per brain vesicle/PPF concentration. Scale bar in A, D, G, J, M, and P = 1 μm; in B, C, E, F, H, I, K, L, N, O, Q, and R = 0,5 μm.

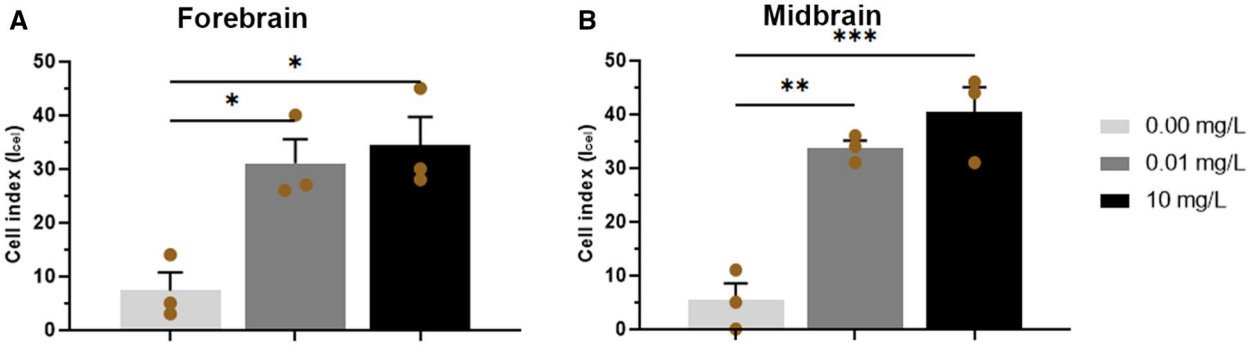

Figure 4. Cell index (I_{cell}) of neural cells in the forebrain (A) and midbrain (B) of *Gallus domesticus* E10 embryos exposed to pyriproxyfen. $n = 3$ brains/36 micrographs-cell per brain/PPF concentration. Mean ± standard error of the mean (SEM). * $p < .05$, ** $p < .01$, *** $p < .001$.

PPF groups, although transcript levels for *vim* decreased in groups exposed to 10 mg/l PPF (0.34 ± 0.03; $p < .001$) and 0.01 mg/l (0.58 ± 0.10; $p < .05$) in relation to control (1.03 ± 0.12). Furthermore, transcript levels for *gfap*, related to differentiation of glial cells, did not differ between groups.

Neuronal cells, except the ependymal layer, were identified in all forebrain and midbrain layers (Figs. 5G–L). In the forebrain, the number of NeuN-positive cells was reduced in the group exposed to 10 mg/l of PPF (1884 positive cells ± 169.90; $p < .05$) compared with control (2994 positive cells ± 141.60). In the

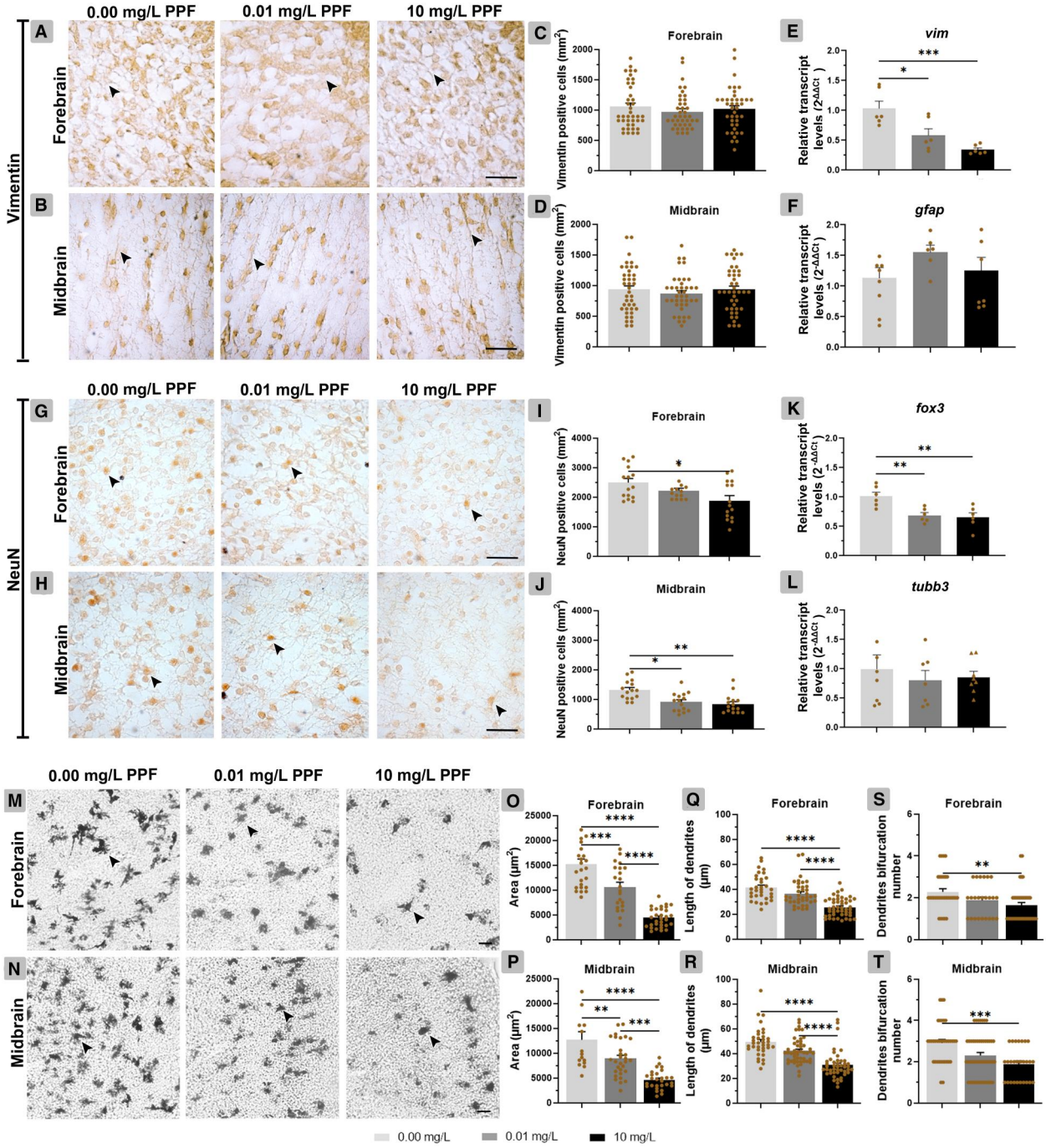

Figure 5. Effect of pyriproxyfen on neural cell differentiation in the forebrain and midbrain of *Gallus domesticus* E10 embryos. (A–D) Cross-sections and graphs of vimentin-positive cells and (H–J) NeuN-positive cells ($n = 3$ brains/PPF concentration). E, F, K, and L, Relative transcript levels of *vim*, *gfap*, *fox3*, and *tubb3* ($n = 9$ brains/PPF concentration). M and N, Cross-sections showing neuronal dendritic branches. O and P, Area occupied by neurons, (Q and R) length of dendritic branches, and (S and T) number of bifurcation dendrites ($n = 6$ brains/PPF concentration). In cross-sections, black arrowhead points for vimentin-positive cells (A, B), NeuN-positive cells (G, H), and neuronal dendritic branches (M, N). Scale bars = 20 µm. Mean ± standard error of the mean (SEM). * $p < .05$, ** $p < .01$, *** $p < .001$, **** $p < .0001$.

midbrain, the number of NeuN-positive cells was decreased in the groups exposed to 10 mg/l PPF (843.40 positive cells ± 83.12; $p < .01$) and 0.01 mg/l (907.60 positive cells ± 80.85; $p < .05$) compared with control (1320 positive cells ± 84.66). The transcript levels for *fox3*, related to mature neurons, reduced in the group exposed to 10 mg/l PPF (0.65 ± 0.07; $p < .01$) and 0.01 mg/l (0.68 ± 0.04; $p < .01$) compared with control (1.01 ± 0.07). The transcript levels for *tubb3*, related to the differentiation of neurons, did not differ between groups.

PPF induced a significant reduction in neuron population in the forebrain and midbrain (Figs. 5M–P). The total area of neurons was reduced in the forebrain of embryos exposed to 10 mg/l PPF (4435 mm^2 ± 340.70; $p < .0001$) and 0.01 mg/l PPF (10 328 mm^2 ± 949.20; $p < .001$) compared with control (15 272 mm^2 ± 1017). The same

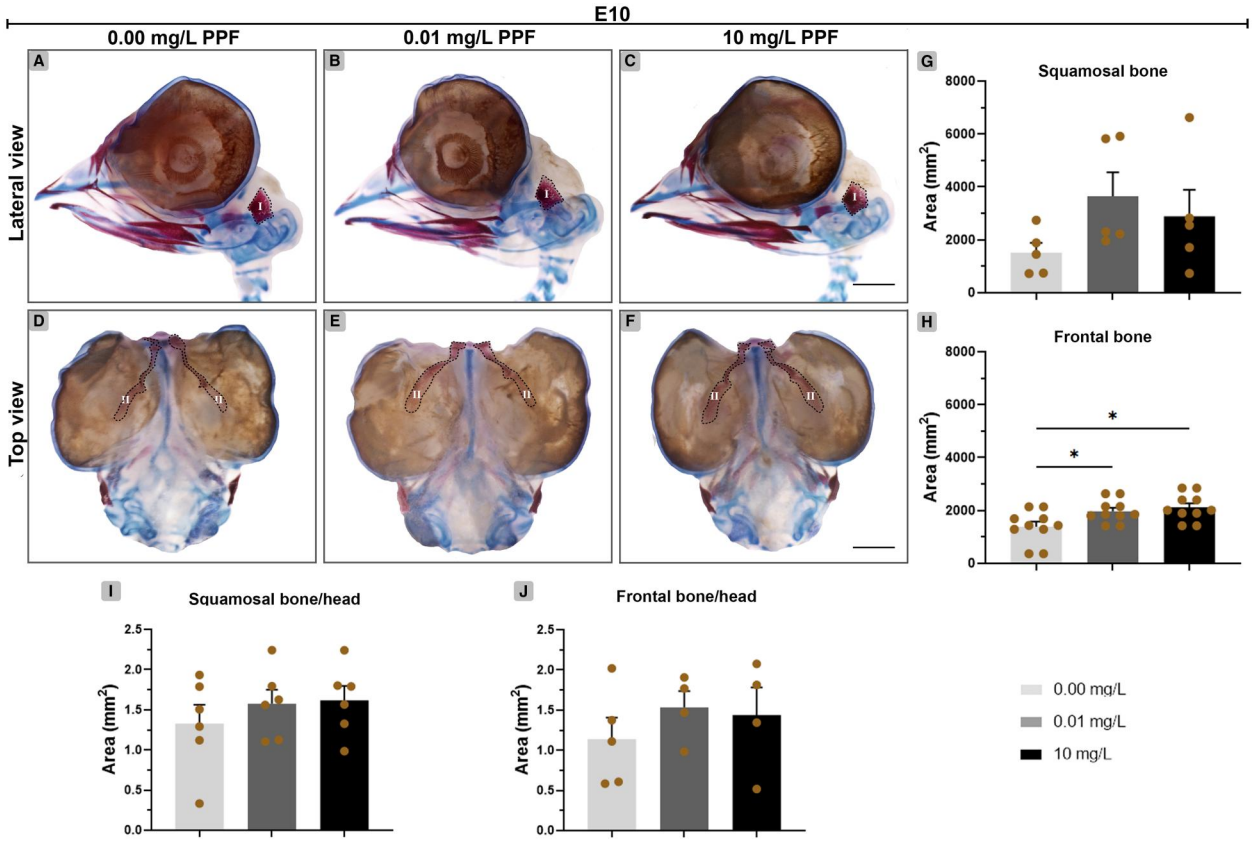

Figure 6. Effect of pyriproxyfen on skull ossification of *Gallus domesticus* E10 embryos. A–F, Heads marked with Alcin blue and Alizarin red. (A–C) Lateral view and (D–F) top view of head. G, H, Bone ossification area. (I, J) Bone-head ratio. I, squamosal; II, frontal. Dashed line indicates bone delimitation. $n = 6$ brains/12 micrographs per brain/PPF concentration. Scale bars in A–F = 1 mm. Mean ± standard error of the mean (SEM). * $p < .05$.

was observed in the midbrain, in the groups exposed to 10 mg/l PPF (4649 mm^2 ± 355.20; $p < .0001$) and 0.01 mg/l PPF (8918 mm^2 ± 663.10; $p < .01$) compared with control (12 693 mm^2 ± 1647).

In the forebrain, a decrease in the length of dendritic branches was observed in the group exposed to 10 mg/l PPF (25.66 µm ± 1.07; $p < .0001$) in relation to control (41.54 µm ± 1.85) (Figs. 5Q–T). Similarly, in the midbrain, the group exposed to 10 mg/l PPF showed a reduction in dendritic branches (30.72 µm ± 1.67; $p < .0001$) compared with control (49.34 µm ± 2.02). The reduction in number of dendrites bifurcations accompanied these reductions. In the forebrain, the group exposed to 10 mg/l PPF (1.64 ± 0.13; $p < .01$) showed a reduction in relation to control (2.28 ± 0.15). Similarly, in the midbrain, the group exposed to 10 mg/l PPF (1.89 ± 0.15; $p < .001$) showed a decrease in dendritic bifurcation compared with control (2.92 ± 0.16).

PPF interferes with head ossification

Regarding the ossification of the head of E10 embryos, the squamosal bone area did not differ between the groups (Figure 6; Supplementary Table 3). In contrast, frontal bone area was greater in E10 embryos exposed to 10 mg/l PPF (2117 mm^2 ±160.30; $p < .001$) and 0.01 mg/l PPF (1973 mm^2 ± 134.50; $p < .01$) compared with control (1386 mm^2 ± 195). The head/squamosal bone and head/frontal bone ratios showed no significant difference between groups.

Later in development, in E15 embryos, the area of the squamosal, frontal, parietal, and supraoccipital bones did not differ in the groups (Figs. 7A–J). The ratio between the head and squamosal bone was higher in the group exposed to 10 mg/l (12 872 mm^2 ± 453.60; $p < .05$) compared with control (10 692 mm^2 ± 350.60) (Figs. 7K–N). The ratio between the head and frontal bone was higher in the group exposed to 10 mg/l (32 115 mm^2 ± 1443; $p < .05$) compared with control (27 315 mm^2 ± 1175). The ratio between the head and parietal or supraoccipital bone showed no significant difference between groups. However, the distance between the frontal bones decreased in embryos exposed to 10 mg/l PPF (149.70 mm ±15.16; $p < .01$), compared with control (214.60 mm ± 7.76) (Figs. 7O–Q). The distance between the frontal and parietal bone also decreased in embryos exposed to 10 mg/l PPF (80.13 mm ± 5.10; $p < .05$) compared with control (117.40 mm ± 7.14). The distance between parietal bones did not differ.

Discussion

Central nervous system congenital anomalies such as microcephaly are responsible for many cases of mental retardation, cerebral palsy, and epilepsy in children worldwide (Mochida, 2009). Understanding the etiology is crucial for identifying prenatal environmental/maternal causes and confirming the diagnosis (Woods and Parker, 2013). Although the impact of toxic substances on the developing central nervous system has been extensively documented, certain substances, such as PPF, remain insufficiently evaluated. Therefore, this study focuses on improving our understanding of the effects of PPF on the developing central nervous system of nontarget organisms and presents new evidence of damage occurring in compartments of neural cells, transcript levels/protein contents related to neural populations, morphological changes in ependyma, and damage to skull ossification.

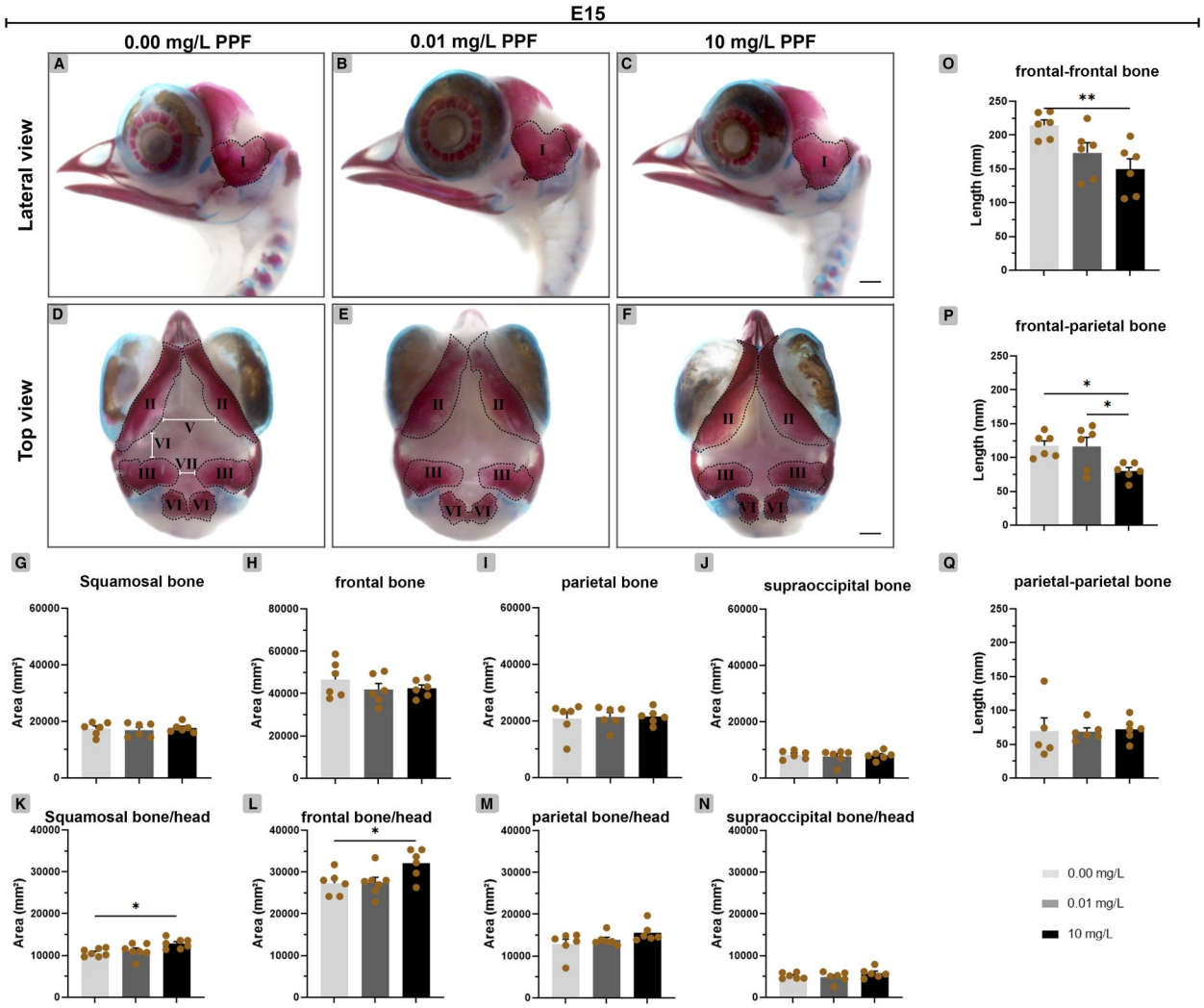

Figure 7. Effect of pyriproxyfen on skull ossification of *Gallus domesticus* E15 embryos. A–F, Heads marked with Alcin blue and Alizarin red. (A–C) Lateral view and (D–F) top view of head. G–J, Bone ossification area. K–N, Bone-head ratio. O–Q, Interbone spacing. I, squamosal; II, frontal; III, parietal; IV, supraoccipital; V, the distance between frontal-frontal bone; VI, the distance between frontal-parietal bone and VII, the distance between parietal-parietal bone. Dashed line indicates bone delimitation. $n = 6$ brains/12 micrographs per brain/PPF concentration. Scale bars in A–F = 2 mm. Mean ± standard error of the mean (SEM). * $p < .05$; ** $p < .01$.

Subcellular analysis indicates that PPF targets cell membranes. The high lipid content of cell membranes promotes the accumulation of lipophilic compounds, such as aromatic hydrocarbons (Backer and Weinstein, 1982). The PPF molecule itself consists of a highly stable aromatic chain (Sullivan and Goh, 2008). It exhibits lipophilic properties (octanol/water partition coefficient—K_{ow}: 5.37), potentially affecting the lipid composition of brain cell membranes (Faria Waziry *et al.*, 2020; Norton *et al.*, 1975). A study using *Xaenopus laevis* observed the bioaccumulation of PPF in lipid-rich structures during the developmental stages of this vertebrate organism (Ose *et al.*, 2017). Incorporating free radicals into the fatty acids of cell membranes could serve as a mechanism by which PPF exerts its effects, leading to structural alterations and metabolic disruptions (Akturk *et al.*, 2006). Biochemical assays have already demonstrated PPF's capacity to increase lipid peroxidation products (Li *et al.*, 2022; Maharajan *et al.*, 2018). Dilatation of the perinuclear space also seems to be a response to toxicity, as it was observed in neural cells in embryos exposed to the highest concentration of PPF. The perinuclear space regulates the traffic of molecules between the nucleus/cytoplasm and modulates several signaling pathways; therefore, changes in this region can directly affect this dynamic (Shaiken and Opekun, 2014).

PPF appears to affect the endoplasmic reticulum and Golgi bodies. Cisternae dilatations in the endoplasmic reticulum can arise due to PPF metabolism, as this organelle plays a role in processing toxic substances (Huang *et al.*, 2022). The action of the PPF could result in the accumulation of misfolded proteins, impeding their transport to the Golgi (Zhang and Kaufman, 2006). Subsequently, cisternae dilatation in the Golgi may lead to increased traffic of secreted vesicles, which may correlate with the observed augmentation in cytoplasmic vacuolation. Cytoplasmic vacuolation is often a reversible mechanism employed by cells to defend against chemical substances (Aki *et al.*, 2012). However, it can also cause irreversible damage to cellular structures such as the endoplasmic reticulum, endosomal-lysosomal system, and Golgi bodies (Henics and Wheatley, 1999; Rogers-Cotrone *et al.*, 2010) and has been associated with neuronal cell death (Krinke *et al.*, 1981). Insecticides are commonly known to induce vacuolation (Henics and Wheatley, 1999), and increased vacuolation in neural cells was observed in newborn mice exposed to 30 mg/

kg PPF (Shahid and Saher, 2020), suggesting this may be a common response to PPF.

Mitochondria appear to be particularly susceptible to the effects of PPF, given the observed damage to their structure, which undoubtedly can impact on their function. The structure of mitochondrial cristae is highly dependent on intracellular Ca^{2+} concentrations, in addition to phospholipids and specific proteins, responsible for anchoring the cristae junction domains to the outer membrane (Bohnert *et al.* 2012; Kondadi *et al.*, 2020; Zerbes *et al.* 2012). Reduced Ca^{2+} transport has been observed in zebrafish brain mitochondria exposed to PPF, indicating disruptions in mitochondrial membrane potential and remodeling of cristae structure (Azevedo *et al.*, 2021; Kowaltowski *et al.*, 2019). Overall, disturbances in mitochondrial homeostasis, as well as that of other organelles, can result in the loss of critical protein interactions involved in vital neurodevelopmental processes, including neuronal differentiation (Robicsek *et al.*, 2013), neuronal migration (Chang *et al.*, 2009), and the growth of dendritic branches (Zuccoli *et al.*, 2023).

The structural modifications, such as decreased neuronal population and branching, and reduced transcript levels and protein contents, suggest disruptions in neural differentiation. PPF induced a decrease in vim transcript levels but did not alter the content of its protein product. The evaluation of vimentin protein content indicates that the quantification primarily reflects an upregulation in gene expression during earlier stages. The observed decrease in *vim* transcript levels could potentially contribute to a subsequent decline in the quantity of vimentin protein at later developmental stages. This data implies that radial glial cells, may become targets of PPF action. PPF does not appear to affect astrocytes and young neurons, as there was no alteration in *gfap* and *tubb3* expression, respectively. The decrease in mature neurons observed here suggests that PPF may affect the cell differentiation mechanism. This suggestion is reinforced by the reduction in NeuN protein content reported in a study by Shahid and Saher (2020) involving prenatal exposure to PPF in rats.

A decrease in the length of dendritic branches induced by exposure to PPF corroborates the cytotoxic effect of some hydrophobic chemicals, such as PPF, which tend to inhibit the growth of dendritic branches (Lee *et al.*, 2022). Changes in the dynamics of the dendritic branching and its bifurcations can directly affect intricate processes such as synaptogenesis, which is vital for the proper development of the central nervous system (Kiyoshi and Tedeschi, 2020). We believe that the reduction of bifurcations and dendritic branches, together with the decrease in neuronal population demonstrated here, can strongly influence cell layer measurements and the size of cerebral vesicles, as demonstrated in our previous work (Luckmann *et al.*, 2021) and in a work by Shahid and Saher (2020).

Ependymal cells showed ultrastructural changes after exposure to PPF. Such exposure apparently enlarged the minor axis of the ependymal cells in midbrain, which consequently increased the area occupied by these cells. The expansion of the cell area may indicate a reduction in cell density in this layer, which has already been documented in a previous study (Luckmann *et al.*, 2021). Already in the forebrain, a decrease in the minor cell axis was observed in embryos exposed to the lower concentration of PPF. It is noteworthy that this reduction may have contributed to the decrease in the area of cilia and microvilli in embryos at the same concentration. However, it was not the sole factor influencing the reduction in the area of these cell surface structures. Upon closer examination of cell surface, it was evident that cilia and microvilli exhibited alterations in their distribution, leading to an increased gap between these structures and consequently reducing the overall occupied area. This impact is particularly relevant as it can directly affect the developmental and physiological processes of the central nervous system (Jiménez *et al.*, 2014), potentially compromising cerebrospinal fluid transport (Rodríguez *et al.*, 2012). Changes in cerebrospinal fluid transit can lead to enlargement of the ventricular cavities and subsequent tissue compression, potentially resulting in a thinner cell layer within the brain without necessarily altering overall brain dimensions (Bruni *et al.*, 1985). Additionally, cerebrospinal fluid plays a role in eliminating toxic substances. It has been found to possess osteoinductive potential in studies involving rats (Klein *et al.*, 1999) and human cerebrospinal fluid (Gautschi *et al.*, 2007). Thus, it is plausible that cerebrospinal fluid serves as a pathway through which PPF gains access to calcium deposition sites, ultimately promoting greater skull ossification. We observed that PPF interferes with the ossification process, as evidenced by decreased inter-bone spacing and increased ossification of specific cranial bones.

Some insecticides used worldwide have been found to affect bone development in different studies. For instance, research by Soni *et al.* (2011) and Sharma *et al.* (2019) indicates that cyfluthrin and endosulfan impact bone development in mice. Additionally, Seleem (2019) found that methomyl affects bone development in tadpoles, and Sekaran *et al.* (2023) discovered similar effects in chick embryos exposed to chlorpyrifos. A plausible explanation for the impact of PPF and other insecticides on ossification may be linked to its influence on growth factors, particularly the bone morphogenetic proteins (BMP), which play a crucial role in promoting the formation of bone and cartilage (Katagiri and Watabe, 2016; Urist and Strates, 1971). Additionally, the cytoskeletal protein gelsolin, known for its regulatory role in BMP signaling pathways (Kanungo *et al.*, 2003), can serve as a target for insecticides. This was demonstrated by Lavastre *et al.* (2002) using toxaphene, which promotes the degradation of this protein. Gelsolin deficiency has been linked to alterations in osteoclast function, which is responsible for bone resorption through demineralization and degradation of the bone matrix (Chellaiah *et al.*, 2000). Consequently, we believe that the observed rise in ossification may be attributed to the inhibition of the typical bone resorption process during osteogenesis.

We demonstrated that the impact on the subcellular compartments of neural cells affects neuronal differentiation processes, leading to decreased neurons. Given the increase in the ossified area observed in the head, it is plausible to propose that the PPF interferes with the normal development of the skull. These findings may directly affect brain measurements, influencing and compromising neurodevelopment. Finally, these data provide new evidence that contributes to understanding the cellular basis of PPF toxicity, and that can be considered in risk assessments by regulatory agencies.

Supplementary data

Supplementary data are available at *Toxicological Sciences* online.

Declaration of conflicting interest

The authors declared no potential conflicts of interest with respect to the research, authorship, and/or publication of this article.

Acknowledgments

The authors are thankful to the Laboratory of Poultry Science (UFSC), the Central Electron Microscopy Laboratory/LCME (UFSC), and the Multiuser Laboratory for Biological Studies/LAMEB (UFSC).

Funding

Scholarships (M.R. Luckmann and M.A.S. Ferreira) of Coordenação de Aperfeiçoamento de Pessoal de Nível Superior (CAPES). E.M. Nazari receives a productivity fellowship of Conselho Nacional de Desenvolvimento Científico e Tecnológico (CNPq - 311570/2020-8).

Author contributions

M.R. Luckmann designed the study, conducted the experiments, analyzed the data, and wrote the manuscript. M.A.S. Ferreira conducted experiments such as exposure of embryos, molecular biology, and histochemical experiments. N.M. Silva analyzed the data and wrote the manuscript. E.M. Nazari designed the study, analyzed the data, wrote the manuscript, and obtained funding. All authors have read and approved the manuscript.

Data availability

The datasets used or analyzed are available from the corresponding author upon reasonable request.

Ethics approval

All experiments were carried out in accordance with the Ethics Committee of UFSC (n° 5843231018/CEUA/UFSC/2018).

References

Aki, T., Nara, A., and Uemura, K. (2012). Cytoplasmic vacuolization during exposure to drugs and other substances. *Cell Biol. Toxicol.* **28**, 125–131.

Akturk, O., Demirin, H., Sutcu, R., Yilmaz, N., Koylu, H., and Altuntas, I. (2006). The effects of diazinon on lipid peroxidation and antioxidant enzymes in rat heart and ameliorating role of vitamin E and vitamin C. *Cell Biol. Toxicol.* **22**, 455–461.

Azevedo, R. D. S., Falcão, K. V. G., Assis, C. R. D., Martins, R. M. G., Araújo, M. C., Yogui, G. T., Neves, J. L., Seabra, G. M., Maia, M. B. S., Amaral, I. P. G., *et al.* (2021). Effects of pyriproxyfen on zebrafish brain mitochondria and acetylcholinesterase. *Chemosphere* **263**, 128029.

Azevedo-Linhares, M., Souza, A. T. C., Lenz, C. A., Leite, N. F., Brito, I. A., Folle, N. M. T., Garcia, J. E., Filipak Neto, F., and Oliveira Ribeiro, C. A. (2018). Microcystin and pyriproxyfen are toxic to early stages of development in *Rhamdia quelen*: An experimental and modelling study. *Ecotoxicol. Environ. Saf.* **166**, 311–319.

Backer, J. M., and Weinstein, I. B. (1982). Interaction of benzo(a)pyrene and its dihydrodiol-epoxide derivative with nuclear and mitochondrial DNA in C3H10T ½ cell cultures. *Cancer Res.* **42**, 2764–2769.

Becerra-Solano, L. E., Mateos-Sánchez, L., and López-Muñoz, E. (2021). Microcephaly, an etiopathogenic vision. *J. Pediatr. Neonatol.* **62**, 354–360.

Bernet, D., Schmidt, H., Meier, W., Burkhardt-Holm, P., and Wahli, T. (1999). Histopathology in fish: Proposal for a protocol to assess aquatic pollution. *J. Fish Dis.* **22**, 25–34.

Bohnert, M., Wenz, L. S., Zerbes, R. M., Horvath, S. E., Stroud, D. A., Von Der Malsburg, K., Müller, J. M., Oeljeklaus, S., Perschil, I., Warscheid, B., *et al.* (2012). Role of mitochondrial inner membrane organizing system in protein biogenesis of the mitochondrial outer membrane. *Mol. Biol. Cell.* **23**, 3948–3956.

Boissy, R. E., Beato, K. E., and Nordlund, J. J. (1991). Dilated rough endoplasmic reticulum and premature death in melanocytes cultured from the vitiligo mouse. *Am. J. Pathol.* **138**, 1511–1525.

Brassier, A., Ottolenghi, C., Boddaert, N., Sonigo, P., Attié-Bitach, T., Millischer-Bellaiche, A. E., Baujat, G., Cormier-Daire, V., Valayannopoulos, V., Seta, N., *et al.* (2012). Prenatal symptoms and diagnosis of inherited metabolic diseases. *Arch. Pediatr.* **19**, 959–969.

Bruni, J. E., Del Bigio, M. R., and Clattenburg, R. E. (1985). Ependyma: Normal and pathological. A review of the literature. *Brain Res.* **356**, 1–19.

Cecchini, M. S., Bourckhardt, G. F., Jaramillo, M. L., Ammar, D., Müller, Y. M. R., and Nazari, E. M. (2019). Exposure to homocysteine leads to cell cycle damage and reactive gliosis in the developing brain. *Reprod. Toxicol.* **87**, 60–69.

Chang, C. J., Yin, P. H., Yang, D. M., Wang, C. H., Hung, W. Y., Chi, C. W., Wei, Y. H., and Lee, H. C. (2009). Mitochondrial dysfunction-induced amphiregulin upregulation mediates chemo-resistance and cell migration in HepG2 cells. *Cell. Mol. Life Sci.* **66**, 1755–1765.

Chellaiah, M., Kizer, N., Silva, M., Alvarez, U., Kwiatkowski, D., and Hruska, K. A. (2000). Gelsolin deficiency blocks podosome assembly and produces increased bone mass and strength. *J. Cell Biol.* **148**, 665–678.

Couly, G. F., Coltey, P. M., and Le Douarin, N. M. (1993). The triple origin of skull in higher vertebrates: A study in quail-chick chimeras. *Development* **117**, 409–429.

Dekkers, M. P., Nikoletopoulou, V., and Barde, Y. A. (2013). Death of developing neurons: New insights and implications for connectivity. *J. Cell Biol.* **203**, 385–393.

De Melo, M. S., dos Santos, T. P. G., Jaramillo, M., Nezzi, L., Rauh Muller, Y. M., and Nazari, E. M. (2019). Histopathological and ultrastructural indices for the assessment of glyphosate-based herbicide cytotoxicity in decapod crustacean hepatopancreas. *Aquat. Toxicol.* **210**, 207–214.

DeSilva, M., Munoz, F. M., Sell, E., Marshall, H., Tse Kawai, A., Kachikis, A., Heath, P., Klein, N. P., Oleske, J. M., Jehan, F., *et al.*; Brighton Collaboration Congenital Microcephaly Working Group. (2017). Congenital microcephaly: Case definition & guidelines for data collection, analysis, and presentation of safety data after maternal immunisation. *Vaccine* **35**, 6472–6482.

Escande-Geraud, M. L., Rols, M. P., Dupont, M. A., Gas, N., and Teissié, J. (1988). Reversible plasma membrane ultrastructural changes correlated with electropermeabilization in Chinese hamster ovary cells. *Biochim. Biophys. Acta.* **939**, 247–259.

Faria Waziry, P. A., Raja, A., Salmon, C., Aldana, N., Damodar, S., Fukushima, A. R., and Mayi, B. S. (2020). Impact of pyriproxyfen on virus behavior: Implications for pesticide-induced virulence and mechanism of transmission. *Virol. J.* **17**, 93.

Fritsche, E., Barenys, M., Klose, J., Masjosthusmann, S., Nimtz, L., Schmuck, M., Wuttke, S., and Tigges, J. (2018). Development of the concept for stem cell-based developmental neurotoxicity evaluation. *Toxicol. Sci.* **165**, 14–20.

Gautschi, O. P., Toffoli, A. M., Joesbury, K. A., Skirving, A. P., Filgueira, L., and Zellweger, R. (2007). Osteoinductive effect of

cerebrospinal fluid from brain-injured patients. *J. Neurotrauma.* **24**, 154–162.

Gilmore, E. C., and Walsh, C. A. (2013). Genetic causes of microcephaly and lessons for neuronal development. *Wiley Interdiscip. Rev. Dev. Biol.* **2**, 461–478.

Hackenbrock, C. R. (1966). Ultrastructural bases for metabolically linked mechanical activity in mitochondria. I. Reversible ultrastructural changes with change in metabolic steady state in isolated liver mitochondria. *J. Cell Biol.* **30**, 269–297.

Henics, T., and Wheatley, D. N. (1999). Cytoplasmic vacuolation, adaptation and cell death: A view on new perspectives and features. *Biol. Cell.* **91**, 485–498.

Huang, Q., Chen, Y., Zhang, Z., Xue, Z., Hua, Z., Luo, X., Li, Y., Lu, C., Lu, A., and Liu, Y. (2022). The endoplasmic reticulum participated in drug metabolic toxicity. *Cell Biol. Toxicol.* **38**, 945–961.

Jiménez, A. J., Domínguez-Pinos, M. D., Guerra, M. M., Fernández-Llebrez, P., and Pérez-Fígares, J. M. (2014). Structure and function of the ependymal barrier and diseases associated with ependyma disruption. *Tissue Barriers.* **2**, e28426.

Juraver-Geslin, H. A., and Durand, B. C. (2015). Early development of the neural plate: New roles for apoptosis and for one of its main effectors caspase-3. *Genesis* **53**, 203–224.

Kanungo, J., Kozmik, Z., Swamynathan, S. K., and Piatigorsky, J. (2003). Gelsolin is a dorsalizing factor in zebrafish. *Proc. Natl. Acad. Sci. U.S.A.* **100**, 3287–3292.

Katagiri, T., and Watabe, T. (2016). Bone morphogenetic proteins. *Cold Spring Harb. Perspect. Biol.* **8**, a021899.

Kiyoshi, C., and Tedeschi, A. (2020). Axon growth and synaptic function: A balancing act for axonal regeneration and neuronal circuit formation in CNS trauma and disease. *Dev. Neurobiol.* **80**, 277–301.

Klein, B. Y., Shohami, E., Reikhinshtein, Y., Ben-Bassat, H., and Liebergall, M. (1999). Serum-mediated osteogenic effects of head injury on cultured rat marrow stromal cells. *Calcif. Tissue Int.* **65**, 217–222.

Kobus, K., Ammar, D., Nazari, E. M., and Rauh Müller, Y. M. (2013). Homocysteine causes disruptions in spinal cord morphology and changes the expression of Pax 1/9 and Sox 9 gene products in the axial mesenchyme. *Birth Defects Res. A Clin. Mol. Teratol.* **97**, 386–397.

Kondadi, A. K., Anand, R., and Reichert, A. S. (2020). Cristae membrane dynamics—A paradigm change. *Trends Cell Biol.* **30**, 923–936.

Kowaltowski, A. J., Menezes-Filho, S. L., Assali, E. A., Gonçalves, I. G., Cabral-Costa, J. V., Abreu, P., Miller, N., Nolasco, P., Laurindo, F. R. M., Bruni-Cardoso, A., *et al.* (2019). Mitochondrial morphology regulates organellar Ca^{2+} uptake and changes cellular Ca^{2+} homeostasis. *Faseb J.* **33**, 13176–13188.

Krinke, G., Schaumburg, H. H., Spencer, P. S., Suter, J., Thomann, P., and Hess, R. (1981). Pyridoxine megavitamninosis produces degeneration of peripheral sensory neurons (sensory neuronopathy) in the dog. *Neurotoxicology* **2**, 13–24.

Lavail, J. H., and Cowan, W. M. (1971). The development of the chick optic tectum. I. Normal morphology and cytoarchitectonic development. *Brain Res.* **28**, 391–419.

Lavastre, V., Roberge, C. J., Pelletier, M., Gauthier, M., and Girard, D. (2002). Toxaphene, but not beryllium, induces human neutrophil chemotaxis and apoptosis via reactive oxygen species (ROS): Involvement of caspases and ROS in the degradation of cytoskeletal proteins. *Clin. Immunol.* **104**, 40–48.

Lee, J., Escher, B. I., Scholz, S., and Schlichting, R. (2022). Inhibition of neurite outgrowth and enhanced effects compared to baseline toxicity in SH-SY5Y cells. *Arch. Toxicol.* **96**, 1039–1053.

Li, X., Naseem, S., Hussain, R., Ghaffar, A., Li, K., and Khan, A. (2022). Evaluation of DNA damage, biomarkers of oxidative stress, and status of antioxidant enzymes in freshwater fish (*Labeo rohita*) exposed to pyriproxyfen. *Oxid. Med. Cell. Longev.* **2022**, 5859266.

Liu, M., Wang, G., Zhang, S. Y., Zhong, S., Qi, G. L., Wang, C. J., Chuai, M., Lee, K. K., Lu, D. X., and Yang, X. (2016). From the cover: Exposing imidacloprid interferes with neurogenesis through impacting on chick neural tube cell survival. *Toxicol. Sci.* **153**, 137–148.

Livak, K. J., and Schmittgen, T. D. (2001). Analysis of relative gene expression data using realtime quantitative PCR and the $2^{-\Delta\Delta Ct}$ method. *Methods* **25**, 402–408.

Luckmann, M. R., de Melo, M. S., Spricigo, M. C., da Silva, N. M., and Nazari, E. M. (2021). Pyriproxyfen exposure induces DNA damage, cell proliferation impairments and apoptosis in the brain vesicles layers of chicken embryos. *Toxicology* **464**, 152998.

Maharajan, K., Muthulakshmi, S., Nataraj, B., Ramesh, M., and Kadirvelu, K. (2018). Toxicity assessment of pyriproxyfen in vertebrate model zebrafish embryos (*Danio rerio*): A multi biomarker study. *Aquat. Toxicol.* **196**, 132–145.

Mall, F. P. (1906). On ossification centers in human embryos less than one hundred days old. *Am. J. Anat.* **5**, 433–458.

Mandarim-de-Lacerda, C. A. (2003). Stereological tools in biomedical research. *An. Acad. Bras. Cienc.* **75**, 469–486.

Mattigk, G. (1989). Overview of the classification and treatment of premature craniosynostosis. On the development of encephalocele following surgery of craniostenosis. *Kinderarztl. Prax.* **57**, 429–433.

Misfeld, M., Szabó, K., Kraatz, E. G., Grossherr, M., Schmidtke, C., Pilgrim, M., Kühnel, W., and Sievers, H. H. (1998). Electron-microscopic findings after transmyocardial laser revascularization in an acute ischemic pig model. *Eur. J. Cardiothorac. Surg.* **13**, 398–403.

Mochida, G. H. (2009). Genetics and biology of microcephaly and lissencephaly. *Semin. Pediatr. Neurol.* **16**, 120–126.

Müller, Y. M. R., Rivero, L. B. D., Carvalho, M. C., Kobus, K., Farina, M., and Nazari, E. M. (2008). Behavioral impairments related to lead-induced developmental neurotoxicity in chicks. *Arch. Toxicol.* **82**, 445–451.

Norton, W. T., Abe, T., Poduslo, S. E., and DeVries, G. H. (1975). The lipid composition of isolated brain cells and axons. *J. Neurosci. Res.* **1**, 57–75.

Olias, P., Adam, I., Meyer, A., Scharff, C., and Gruber, A. D. (2014). Reference genes for quantitative gene expression studies in multiple avian species. *PLoS One.* **9**, e99678.

Opitz, J. M., and Holt, M. C. (1990). Microcephaly: General considerations and aids to nosology. *J. Craniofac. Genet. Dev. Biol.* **10**, 175–204.

Ose, K., Miyamoto, M., Fujisawa, T., and Katagi, T. (2017). Bioconcentration and metabolism of pyriproxyfen in tadpoles of African clawed frogs, *Xenopus laevis*. *J. Agric. Food Chem.* **65**, 9980–9986.

Passemard, S., Kaindl, A. M., and Verloes, A. (2013). Microcephaly. *Handb. Clin. Neurol.* **111**, 129–141.

PubChem. (2023). *PubChem Compound Summary for CID 91753, Pyriproxyfen.* National Center for Biotechnology Information. Available at: https://pubchem.ncbi.nlm.nih.gov/compound/Pyriproxyfen. Retrieved February 9, 2023.

Radulescu, A. E., Siddhanta, A., and Shields, D. (2007). A role for clathrin in reassembly of the Golgi apparatus. *Mol. Biol. Cell.* **18**, 94–105.

Robicsek, O., Karry, R., Petit, I., Salman-Kesner, N., Müller, F. J., Klein, E., Aberdam, D., and Ben-Shachar, D. (2013). Abnormal neuronal differentiation and mitochondrial dysfunction in hair

follicle-derived induced pluripotent stem cells of schizophrenia patients. *Mol. Psychiatry*. **18**, 1067–1076.

Rodríguez, E. M., Guerra, M. M., Vío, K., González, C., Ortloff, A., Bátiz, L. F., Rodríguez, S., Jara, M. C., Muñoz, R. I., Ortega, E., *et al.* (2012). A cell junction pathology of neural stem cells leads to abnormal neurogenesis and hydrocephalus. *Biol. Res.* **45**, 231–242.

Rogers-Cotrone, T., Burgess, M. P., Hancock, S. H., Hinckley, J., Lowe, K., Ehrich, M. F., and Jortner, B. S. (2010). Vacuolation of sensory ganglion neuron cytoplasm in rats with long-term exposure to organophosphates. *Toxicol. Pathol.* **38**, 554–559.

Ross, J. (1993). *Microcephaly Handbook of Clinical Neurology*, Vol. **30**. Elsevier, Amsterdam.

Röth, E., Szmolenszky, T., and Török, E. (1980). Ultrastructural features of canine kidneys after preservation with hyperthermic solutions and subsequent reperfusion. *Int. Urol. Nephrol.* **12**, 137–151.

Sanzo, J. F., and Tuan, R. S. (1998). High sensitivity analysis of gene expression in single embryonic somites using coupled reverse transcription-polymerase chain reaction. *Mol. Biotechnol.* **9**, 7–15.

Sarnat, H. B., and Flores-Sarnat, L. (2002). What's new in neuroembryology? Cajal–Retzius and subplate neurons: Their role in cort ical development. *Eur. J. Paediatr. Neurol.* **6**, 91–97.

Saunders, N. R., Liddelow, S. A., and Dziegielewska, K. M. (2012). Barrier mechanisms in the developing brain. *Front. Pharmacol.* **3**, 46.

Sekaran, S. P. C., Thotakura, B., Jyothi, A. K., Manickam, S., Chanemougavally, J., Prabhu, K., and Gopalan, D. H. (2023). Effect of chlorpyrifos and its metabolites on skeletal system development of chick embryo. *Birth Defects Res.* **115**, 1063–1078.

Seleem, A. A. (2019). Teratogenicity and neurotoxicity effects induced by methomyl insecticide on the developmental stages of *Bufo arabicus*. *Neurotoxicol. Teratol.* **72**, 1–9.

Shahid, A., and Saher, M. (2020). Repeated exposure of pyriproxyfen to pregnant female mice causes developmental abnormalities in prenatal pups. *Environ. Sci. Pollut. Res. Int.* **27**, 26998–27009.

Shaiken, T., and Opekun, A. (2014). Dissecting the cell to nucleus, perinucleus and cytosol. *Sci. Rep.* **4**, 4923.

Sharma, A., John, P. J., and Bhatnagar, P. (2019). Combination of fluoride and endosulfan induced teratogenicity and developmental toxicity in Swiss albino mice exposed during organogenesis. *Toxicol. Ind. Health.* **35**, 604–613.

Soni, I., Syed, F., Bhatnagar, P., and Mathur, R. (2011). Perinatal toxicity of cyfluthrin in mice: Developmental and behavioral effects. *Hum. Exp. Toxicol.* **30**, 1096–1105.

Sullivan, J. J. S., and Goh, K. S. G. (2008). Environmental fate and properties of pyriproxyfen. *J. Pest. Sci.* **33**, 339–350.

Truong, L., Gonnerman, G., Simonich, M. T., and Tanguay, R. L. (2016). Assessment of the developmental and neurotoxicity of the mosquito control larvicide, pyriproxyfen, using embryonic zebrafish. *Environ. Pollut.* **218**, 1089–1093.

Urist, M. R., and Strates, B. S. (1971). Bone morphogenetic protein. *J. Dent. Res.* **50**, 1392–1406.

Whetsell, W. O., Jr, and Bunge, R. P. (1969). Reversible alterations in the Golgi complex of cultured neurons treated with an inhibitor of active Na and K transport. *J. Cell Biol.* **42**, 490–500.

WHO. (2006). *Pesticides and Their Application for the Control of Vectors and Pests of Public Health Importance*, 6th ed. World Health Organization, Geneva.

WHO. (2020). *The WHO Recommended Classification of Pesticides by Hazard and Guidelines to Classification 2019*. World Health Organization, Geneva.

Woods, C. G., Bond, J., and Enard, W. (2005). Autosomal recessive primary microcephaly (MCPH): A review of clinical, molecular, and evolutionary findings. *Am. J. Hum. Genet.* **76**, 717–728.

Woods, C. G., and Parker, A. (2013). Investigating microcephaly. *Arch. Dis. Child.* **98**, 707–713. 2012.

Zerbes, R. M., Bohnert, M., Stroud, D. A., Von Der Malsburg, K., Kram, A., Oeljeklaus, S., Warscheid, B., Becker, T., Wiedemann, N., Veenhuis, M., *et al.* (2012). Role of MINOS in mitochondrial membrane architecture: Cristae morphology and outer membrane interactions differentially depend on mitofilin domains. *J. Mol. Biol.* **422**, 183–191.

Zhang, K., and Kaufman, R. J. (2006). The unfolded protein response a stress signaling pathway critical for health and disease. *Neurology* **66**, S102–109.

Zuccoli, G. S., Nascimento, J. M., Moraes-Vieira, P. M., Rehen, S. K., and Martins-de-Souza, D. (2023). Mitochondrial, cell cycle control and neuritogenesis alterations in an iPSC-based neurodevelopmental model for schizophrenia. *Eur. Arch. Psychiatry Clin. Neurosci.* **273**, 1649–1664.